Cellular senescence in vascular wall mesenchymal stromal cells, a possible contribution to the development of aortic aneurysm

Gabriella Teti [a],[*], Francesca Chiarini [b],[c], Eleonora Mazzotti [d], Alessandra Ruggeri [a], Francesco Carano [a], Mirella Falconi [a]

[a] Department of Biomedical and Neuromotor Sciences, University di Bologna, Bologna, 40126, Italy
[b] CNR-National Research Council of Italy, Institute of Molecular Genetics "Luigi Luca Cavalli-Sforza", Unit of Bologna, Bologna, 40136, Italy
[c] IRCCS Istituto Ortopedico Rizzoli, Bologna, 40136, Italy
[d] Faculty of Bioscience and Agro-Food and Environmental Technology, University of Teramo, Teramo, 64100, Italy

ARTICLE INFO

ABSTRACT

Cellular senescence is a hallmark of ageing and it plays a key role in the development of age-related diseases. Abdominal aortic aneurysm (AAA) is an age related degenerative vascular disorder, characterized by a progressive dilatation of the vascular wall and high risk of rupture over time. Nowadays, no pharmacological therapies are available and the understanding of the molecular mechanisms that lead to AAA onset and development are poorly defined.

In this study we investigated the cellular features of senescence in vascular mesenchymal stromal cells, isolated from pathological (AAA – MSCs) and healthy (h – MSCs) segments of human abdominal aorta and their implication in impairing the vascular repair ability of MSCs.

Cell proliferation, ROS production, cell surface area, the expression of cyclin dependent kinase inhibitors p21^{CIP1} and p16^{INK4a}, the activation of the DNA damage response and a dysregulated autophagy showed a senescent state in AAA - MSCs compared to h-MSCs. Moreover, a reduced ability to differentiate toward endothelial cells was observed in AAA – MSCs.

All these data suggest that the accumulation of senescent vascular MSCs over time impairs their remodeling ability during ageing. This condition could support the onset and development of AAA.

1. Introduction

Cellular senescence is classified as an irreversible growth arrest of the cell cycle and alteration of the gene expression profile resulting from a variety of stresses, such as DNA mutation, reactive oxygen species (ROS) and telomere shortening (Hernandez-Segura et al., 2018; Regulski, 2017). Senescent cells accumulate during ageing. A great deal of evidence suggests a strong involvement of senescent cells in several age-related diseases (Katsuumi et al., 2018; López-Otín et al., 2013).

In heart failure the presence of senescent endothelial cells has been reported as inductors of pathological changes in the failing heart (Shimizu and Minamino, 2019; Ungvari et al., 2020Figure 7; Ungvari et al., 2018). Vascular smooth muscle cells and senescent endothelial cells have been observed in the atherosclerotic plaque and playing a key role in the progression of plaque (Ungvari et al., 2020; Shimizu and

Minamino, 2019; Ungvari et al., 2018).

Vascular tissue remodeling occurs with ageing. Aged arteries are characterized by the increase of the intima/media thickness ratio. Vascular smooth muscle cells, change from a "contractile" to a "synthetic" phenotype, losing their cellularity. Furthermore, tunica media participates in increasing the intimal layer and it is associated to an increase of the vascular permeability (Ungvari et al., 2018). In association with the morphological and functional changes in aged arteries, the presence of medial calcification is another quite representative characteristic of aged vessels (Katsuumi et al., 2018).

Abdominal aortic aneurysm (AAA) corresponds to a weakening of the abdominal aorta wall followed by a dilation over years. The main complication is the rupture of the abdominal wall which leads to death. It is usually asymptomatic, and during screening programmers for other unrelated pathologies it is frequently diagnosed (Golledge, 2019;

---

* Corresponding author at: Department of Biomedical and Neuromotor Sciences (DIBINEM), University of Bologna, Section of Human Anatomy, Via Irnerio, 48, Bologna, 40126, Italy.
E-mail address: gabriella.teti2@unibo.it (G. Teti).

Schmitz-Rixen et al., 2016). Open or minimally invasive surgery is the most common treatment for AAA, but its applicability to less fit patients is complex and post-surgery AAA ruptures are possible (Badger et al., 2017; Ballard et al., 2000).

No pharmacological treatment is available for small asymptomatic AAA, and the current suggested guidelines are based on monitoring AAA diameters and symptoms over time (Golledge, 2019).

The pathogenesis of AAA is believed to be the consequence of a combination of inherited and environmental factors, which activate the inflammatory reaction. Atherosclerosis often contributes to the progression of AAA (Bernal et al., 2020; Golledge, 2019; Peshkova et al., 2016).

Aged arteries are characterized by the presence of accumulation of senescent endothelial and senescent vascular smooth cells, in association with high levels of ROS, cyclin dependent kinase (CdK) inhibitors

p16[INK4a] and p21[CIP1], phosphorylated p38, double stranded DNA breaks and high SA-β-Gal activity (Jia et al., 2019; Ungvari et al., 2018; Hernandez-Segura et al., 2018). Furthermore, these cells are also accumulated in the vessels of patients with atherosclerorsis (Shimizu and Minamino, 2019), hypertension (McCarthy et al., 2019), diabetes (Berlanga-Acosta et al., 2020) and intimal hyperplasia (Ungvari et al., 2018). In particular, in patients with AAA, endothelial cells and vascular smooth muscle cells showed telomeres significantly shorter and oxidative DNA damage compared to healthy elderly persons (Bautista-Niño et al., 2016).

Vascular, resident stem cells are present in all 3 layers of the vessel wall. Endothelial precursor cells (EPCs), smooth muscle precursors cells (SMPCs) and mesenchymal stromal/stem cells (MSCs), have been widely demonstrated in the intima, neointima, media and adventitia tunica of blood vessels (Zhang et al., 2018; Lu and Li, 2018; Psaltis et al., 2011;).
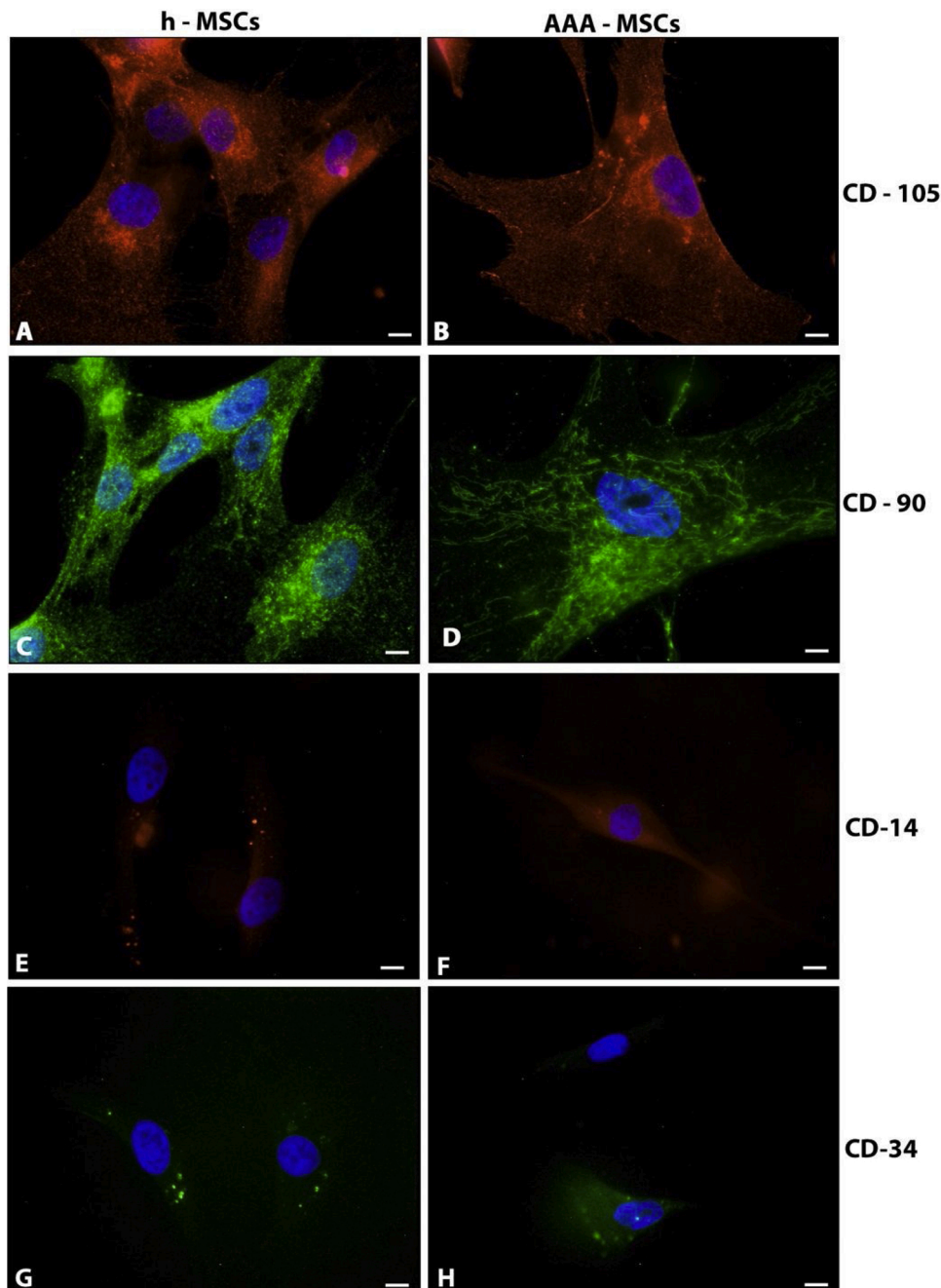

Fig. 1. representative images of h – MSCs (A, C, E and G) and AAA – MSCs (B, D, F and H) immunolabeled for CD105 (1A and 1B), CD90 (1C and 1D) mesenchymal stromal markers and CD14 (1E and 1 F) and CD34 (1 G and 1 H) hematopoietic markers. Cells isolated from all the patients were positive for both the mesenchymal stromal markers and they were negative for both the hematopoietic markers. CY3 conjugated secondary antibody was used to detect the fluorescence signal of CD105 and CD14 markers while Alexa Fluor 488 conjugated secondary antibody was used to detect the fluorescence signal of CD90 and CD34 markers. All the samples were counterstained with DAPI (magnification: 600X; bar: 100 nm).

They play a role in vascular formation under remodeling in physiological and pathological conditions (Zhang et al., 2018; Psaltis and Simari, 2015). Among them, MSCs with angiogenic abilities, have been demonstrated (Ciavarella et al., 2015). MSCs are endowed with self-renewal and, under the appropriate stimulation, are able to differentiate into multiple cell types along the mesodermal lineage (adipocytes, chondrocytes, osteocytes) (Mattioli-Belmonte et al., 2015; Focaroli et al., 2014; Teti et al., 2012; Caplan, 2007). Thanks to these properties, MSCs regulate many reparative processes in the presence of tissue damage as well as keep the tissue homeostasis under physiologic conditions (Mazzotti et al., 2019; Teti et al., 2018; Focaroli et al., 2016). Widely studied for their immunomodulatory and anti-inflammatory properties (Ahangar et al., 2020; Harrell et al., 2020), MSCs showed impaired differentiation abilities and reduced anti-inflammatory properties when isolated by pathological tissues (Banimohamad-Shotorbani et al., 2020). Previous studies demonstrated matrix metalloproteinase 9 (MMP9) upregulation in MSCs isolated from the aortic wall of AAA patients (Ciavarella et al., 2015), and a reduced ability to secrete anti-inflammatory molecules (Lunyak et al., 2017).

In adults, the vascular stem cells are mostly quiescent in their niches but can be activated in response to injury and participate in endothelial repair and smooth muscle cell accumulation to form neointima (So and Cheung, 2018; Terzi et al., 2016). Genetic or environmental risk factors that lead to hypertension, hyperlipidemia, hyperglycemia, systemic inflammation, circulation of ROS, among other conditions can cause endothelial injury and dysfunction. As a result, vascular cell, including stem/ progenitor cell, migration, proliferation, and differentiation are affected (Mohammad et al., 2019). Vessel injuries should activate progenitor vascular stem cells triggering a vascular remodeling process but during ageing the molecular mechanisms are not properly activated (Ungvari et al., 2018).

Our hypothesis is that, during ageing progenitor vascular MSCs could have accumulated damages inducing cellular senescence which weaken their reparative abilities.

The purpose of this study is to demonstrate the presence of cellular senescence in vascular MSCs of AAA (AAA – MSCs), responsible of an impaired vascular remodeling process. MSCs isolated from the vascular wall of AAA, were assayed for their proliferative ability, cellular senescence markers, autophagy and in vitro vascular differentiation. The results were compared to MSCs isolated from healthy segment of the abdominal aorta of the same patients (h – MSCs).

2. Experimental procedures

2.1. AAA sample collection and MSCs isolation

AAA samples were collected in collaboration with the Unit of Vascular Surgery, "Santa Maria delle Croci" Ravenna Hospital, from 3 patients (2 male and 1 female), during repair surgery following the guidelines of the Ethics Committee of Ravenna Hospital and in accordance with The Code of Ethics of the World Medical Association. Healthy samples of abdominal aorta consist in the most external segments of the removed pathological aorta, adjacent to the aneurismatic regions. Abdominal aorta explants were dissected in small pieces (3−4 mm^3), cultured in Minimal essential medium (MEM) (Gibco, Thermo Scientific, Monza, Italia) supplemented with 10 % fetal calf serum (FCS) (Gibco, Thermo Scientific, Monza, Italia) at 37 °C in a humidified atmosphere of 5% CO_2. Cells obtained from AAA (AAA-MSCs) and healthy (h-MSCs) explants, from passage 2–5, were utilized for the following experiments.

2.2. Immunofluorescence microscopy for MSC marker detection

The expression of CD105, CD90, surface mesenchymal markers and of CD14 and CD34, hematopoietic markers, was investigated by immunofluorescence on AAA-MSCs and h-MSCs. Cells were seeded on

glass slides at the density of 20.000 cells /glass and cultured for three days under the culture condition previously described. Then, the samples were washed in PBS and fixed with 4% paraformaldehyde in phosphate buffer saline (PBS) containing 0.1 % Triton - X 100 (Sigma Aldrich, St. Louis, Missouri, USA) at 4 °C and for 30 min, washed in PBS and treated with a solution of 2.5 % bovine serum albumin (BSA) (Sigma Aldrich, St. Louis, Missouri, USA) in PBS (blocking reagent) per 30 min at room temperature (RT).

Glasses were subsequently incubated over night at 4 °C with the following primary antibodies: mouse anti- human CD105 diluted 1:100 (Thermo Fisher Scientific, Monza, Italy), rabbit anti- human CD90 (Thermo Fisher Scientific, Monza, Italy) diluted 1:500, mouse anti-human CD14 diluted 1:100 (Thermo Fisher Scientific, Monza, Italy) and rabbit anti-human CD34 diluted 1:100 (Thermo Fisher Scientific, Monza, Italy). All the primary antibodies were diluted in blocking reagent. After three washes in 0.1 %Tween 20 in PBS (PBS-T), the samples were incubated for 1 h and 30 min at 37 °C with secondary antibodies anti-mouse IgG – Cy3 conjugated (Sigma Aldrich, St. Louis, Missouri, USA), and anti-rabbit IgG Alexa Fluor 488 conjugated (Cell Signaling Technology), both diluted 1:2000 in PBS. After rinsing in PBS the samples were counterstained with DAPI, mounted in Vectashield anti-fade medium (Vector Laboratories, Inc, Burlingame, CA, USA) and observed under a fluorescence microscopy Eclipse E800 Nikon (Nikon,
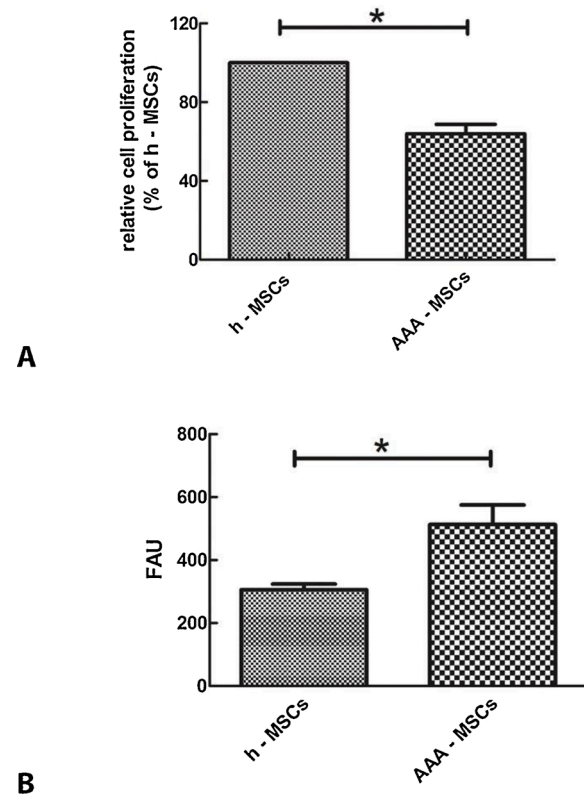

Fig. 2. (A) BrdU proliferation assay showing a reduced proliferation of AAA – MSCs compared to h – MSCs. For each experimental group the results are the average value obtained from cells of each donor, and they are expressed as relative cell proliferation compared to h - MSCs. Each individual assay was performed in triplicates and expressed as mean of percentage ± SD. * represents a significant difference compared to h - MSCs, p < 0.05. (B) Intracellular ROS of h – MSCs and AAA – MSCs were measured by using carboxy-H$_2$DCFDA and results were expressed in fluorescent arbitrary units (FAU). For each experimental group the results are the average value, obtained from cells of each donor. Each individual assay was performed in triplicates and expressed as mean value ± SD. * represents a significant difference compared to h - MSCs, p < 0.05.

Tokyo, Japan). Negative controls consisted in h-MSCs and AAA – MSCs incubated with the secondary antibody anti-mouse IgG – Cy3 conjugated (Sigma Aldrich, St. Louis, Missouri, USA), and anti-rabbit IgG Alexa Fluor 488 conjugated (Cell Signaling Technology), diluted 1:2000 in PBS, for 1 h and 30 min at 37 °C. Samples were then processed as previously described. Results were shown in the supplementary file (Fig. 1).

2.3. BrdU proliferation assay

Cell proliferation was tested by BrdU assay kit (Roche, Basel, Switzerland) according to the manufacturer's instructions. Briefly, cells were seeded into a 96-well culture plate with DMEM containing 10 % FBS in a density of 10^4 cells/well. After 24 h, the medium was changed to a fresh one containing 10 μM BrdU for 96 h at 37 °C. At the end of the treatment, the cells were fixed and incubated with anti-BrdU antibody conjugated with peroxidase for 90 min at RT. After three washes in PBS, a tetramethyl–benzidine (TMB) substrate solution was added for 20 min at RT, and the reaction was stopped with 1 M H_2SO_4. The optical density was measured using a spectrophotometer Microplate Reader (LT-4000, LabTech, Euroclone, Milan, Italy) at a wavelength of 450 nm and a reference wavelength of 690 nm. Results were expressed in percentage as relative values compared to h-MSCs.

2.4. ROS detection assay

6-carboxy-2′,7′-dichlorodihydrofluorescein diacetate (carboxy-H_2DCFDA) fluorescent labeling was used to measure the total intracellular production of ROS in AAA – MSCs and h – MSCs. For the procedure, 10^4 cells/well were seeded into a 96-well culture plate in MEM containing 10 % FBS. After 24 h, the medium was changed to a fresh one containing 5μM carboxy-H_2DCFDA, ROS detection probe (Thermo Fisher Scientific, Monza, Italy), for 3 h at 37 °C. As positive control, the same samples were treated with 200 mM of H_2O_2 in DMEM for 2 h at 37 °C (data not showed). The fluorescent signal was measured using a fluorimeter microplate reader (Glomax, Promega Corporation, Madison, WI, USA) at a fluorescence excitation of 492 nm and at fluorescence emission of 517 nm.

2.5. vascular MSC surface area

The F-actin staining procedure was performed according to the manufacturer's instructions (Molecular Probes, Invitrogen, Eugene, OR). The assay is based on the high binding affinity of a fluorescent bicyclic peptide, phallotoxin, toward actin filament. Briefly, cells were seeded on glass slides at the density of 20.000 cells /glass in MEM supplemented with 10 % FBS at 37 °C for 24 h. Then, samples were fixed in 4% paraformaldehyde in PBS for 20 min at 4 °C and subsequently
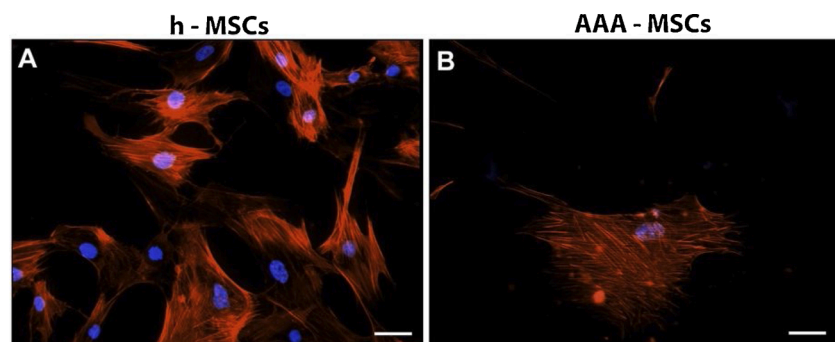

Fig. 3. representative fluorescent images of h – MSCs (A) and AAA – MSCs (B) labeled with the fluorescent Phalloidin probe, selective for the F- actin protein. A more disorganized distribution of actin filaments is observed in AAA – MSCs compared to h – MSCs. All the samples were counterstained with DAPI (magnification: 200X; bar: 20 μm). (E) Quantitative analysis of cellular area expressed as fold increase compared to h – MSCs. For each experimental group the results are the average value, obtained from cells of each donor. F-actin staining assay was performed in duplicate and the relative quantification was expressed as mean value ± SD. * represents a significant difference compared to h - MSCs, p < 0.05.
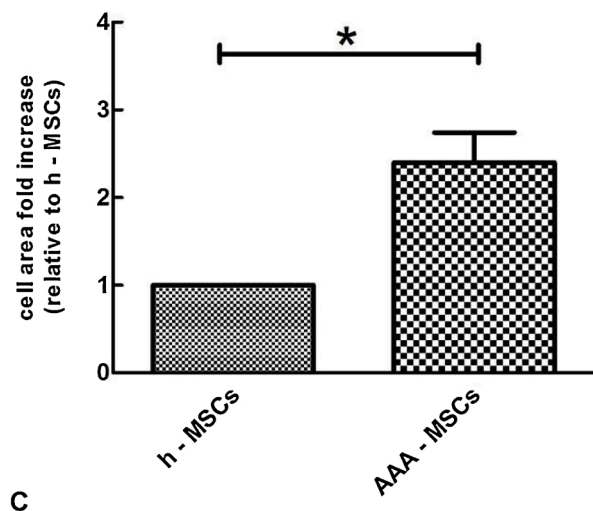
permeabilized by 0.1 % Triton – X in PBS for 5 min at RT. Coverslips were stained with fluorescent phalloxin diluted to 1:40 in 1% BSA for 20 min at RT. After three washes in PBS and distilled water, coverslips were counterstained with DAPI and then mounted with the permanent mountant ProLong gold (Invitrogen, Thermo Fisher Scientific, Waltham, Massachusetts, USA). Images were acquired by the fluorescence microscope Eclipse E800 (Nikon, Tokyo, Japan).

The quantitative analysis of phalloxin-stained areas was assessed by measuring cellular area in at least 20 cells for each sample, from acquired images corresponding to different fields for each slide at 20X magnification. The quantitative analysis was performed by the Leica Qwin 3.0 software (Leica Microsystems Srl, Cambridge, UK), which allowed the phalloxin-stained area to be selected and measured.

2.6. Western blot analysis

Cellular pellets of AAA-MSCs and h-MSCs were extracted by using RIPA lysis buffer (Pierce, Thermo Fisher Scientific, Monza, Italy) supplemented with 25 µmol/L protease inhibitor cocktail (Pierce, Thermo Fisher Scientific, Monza, Italy) and 1 µL of β-mercapto-ethanol (Sigma-Aldrich, St. Louis, Missouri, USA). Total proteins were resolved on 4–12 % SDS polyacrylamide gel electrophoresis (SDS–PAGE) and electrophoretically transferred onto a nitrocellulose membrane using a wet blotting apparatus (Invitrogen, Thermo Fisher Scientific, Monza, Italy). The membranes were blocked with dry milk (blocking reagent) (Invitrogen, Thermo Fisher Scientific, Monza, Italy) for 30 min at room temperature and were then incubated with the following primary antibodies:

mouse anti-human p53 antibody (Cell Signaling Technologies, Euroclone, Milan, Pero); mouse anti-human phospho - p53 (Ser 15) (Cell Signaling Technologies, Euroclone, Milan, Italy); rabbit anti-human p21^{CIP} antibody (Cell Signaling Technologies, Euroclone, Milan, Italy); rabbit anti human p16^{INK4A} antibody (Cell Signaling Technologies, Euroclone, Milan, Italy); rabbit anti-human Beclin (Cell Signaling Technologies, Euroclone, Milan, Italy); rabbit anti-human LC3 (Cell Signaling Technologies, Euroclone, Milan, Italy); mouse anti-human tubulin antibody (Sigma- Aldrich, St Louis, Missouri, USA) and mouse anti-human actin antibody (Millipore Merck, Darmstadt, Germany).

All the primary antibodies were diluted 1:1000 in blocking reagent and the incubations were performed at 4 °C over night. After washing with TBS-Tween buffer, each blot was incubated with anti-rabbit secondary antibody (1:2000 dilution; Cell Signaling Technology, Euroclone, Milan, Italy) or anti-mouse antibody (1:2000 dilution; Sigma Aldrich, St Louis, Missouri, USA) for 1 h and 30 min at room temperature. The antibody signal was visualized with the enhancement chemiluminescence system (Pierce, Thermo Fisher Scientific, Monza, Italy). Images were obtained by using IBright Western Blot Imaging System (Thermo Fisher Scientific, Massachusetts, USA). Band densitometry was determined using ImageJ software (National Institutes of Health), and the intensities of the specific protein bands were corrected for equal tubulin loading (or actin loading); they were expressed as relative to the intensity of the control sample (h-MSCs). Data showed the average of triplicates $\pm$ SD and were representative from three independent experiments.
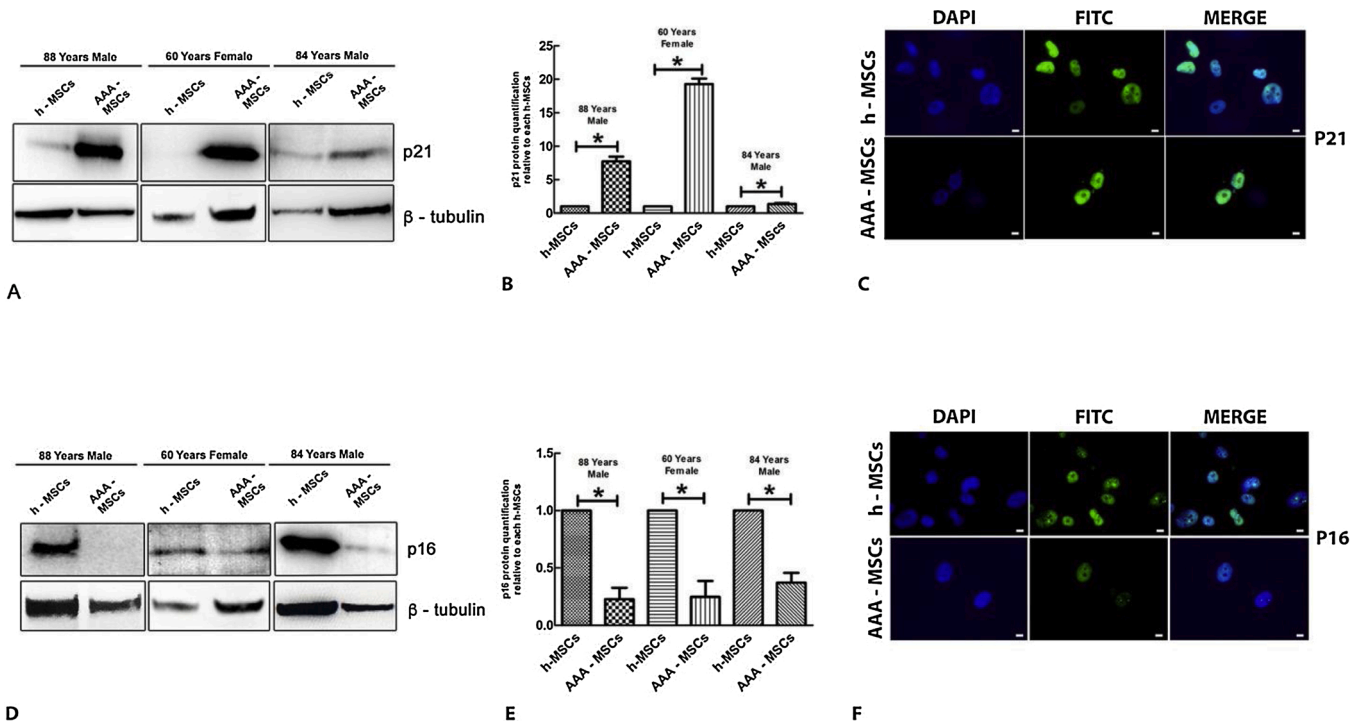

Fig. 4. (A) representative western blot images showing p21^{CIP1} expression in h – MSCs and AAA – MSCs. Results from cells of each donor were shown. (B) Relative amounts of p21^{CIP1} expression were normalized to the intensity of β-tubulin and represented as fold increase relative to h – MSCs of each donor. Western blot was performed in duplicate and the relative quantification was expressed as mean value $\pm$ SD. * represents a significant difference compared to h - MSCs, $p < 0.05$. (C) immunofluorescence detection of p21^{CIP1} in h – MSCs and AAA – MSCs. Alexa Fluor 488 conjugated secondary antibody was used to detect the fluorescence signal of p21^{CIP1}. All the samples were counterstained with DAPI (magnification 600X; bar: 100 nm). (D) representative western blot images showing p16^{INK4a} expression in h – MSCs and AAA – MSCs. Results from each donor were shown. (E) Relative amounts of p16^{INK4a} expression were normalized to the intensity of β-tubulin and represented as fold decrease relative to h – MSCs of each donor. Western blot was performed in duplicate and the relative quantification was expressed as mean value $\pm$ SD. * represents a significant difference compared to h - MSCs, $p < 0.05$. (F) immunofluorescence detection of p16^{INK4a} in h – MSCs and AAA – MSCs. Alexa Fluor 488 conjugated secondary antibody was used to detect the fluorescence signal of p16^{INK4a}. All the samples were counterstained with DAPI (magnification: 600X; bar: 100 nm).

2.7. Immunofluorescence microscopy

AAA-MSCs and h-MSCs were seeded on glass slides at the density of 20.000 cells /glass and cultured for three days under the culture condition previously described. Then, the samples were washed in PBS and fixed with 4% paraformaldehyde in phosphate buffer saline (PBS) containing 0.1 % Triton - X 100 (Sigma Aldrich, St. Louis, Missouri, USA) at 4 °C and for 30 min, washed in PBS and treated with a solution of 2.5 % bovine serum albumin (BSA) (Sigma Aldrich, St. Louis, Missouri, USA) in PBS (blocking reagent) per 30 min at room temperature (RT).

Glasses were subsequently incubated over night at 4 °C with the following primary antibodies:

rabbit anti-human phospho-Histone H2A.X antibody diluted 1:200 (Invitrogen, Thermo Fisher Scientific, Monza, Italy); rabbit anti-human p21^{CIP1} antibody (Cell Signaling Technologies, Euroclone, Milan, Italy) diluted 1:1000 and rabbit anti human p16^{INK4a} antibody (Cell Signaling Technologies, Euroclone, Milan, Italy) diluted 1:1000. After several washes in PBS-T, the samples were incubated for 1 h and 30 min at 37 °C with secondary antibody anti-rabbit IgG Alexa Fluor 488 conjugated (Cell Signaling Technology) diluted 1:2000 in PBS. After rinsing in PBS the samples were counterstained with DAPI, mounted in vectashield medium (Vector Laboratories, Inc, Burlingame, CA, USA) and observed under a fluorescence microscopy Eclipse E800 Nikon (Nikon, Tokyo, Japan).

2.8. Transmission Electron Microscopy

AAA-MSCs and h-MSCs were seeded on cover glasses at the density of 20.000 cells/glass and cultured as previously described. After 24 h, the cells were fixed in 2.5 % glutaraldehyde in 0.1 M phosphate buffer for 2 h and post-fixed in 1% OsO$_4$ in 0.1 M phosphate buffer for 1 h at 4 °C. Then, the samples were dehydrated in a graded series of aceton and embedded in Epon resin (Sigma Aldrich, St. Louis, Missouri, USA). Ultrathin sections were counterstained with uranyl acetate and lead citrate and observed under a Philips CM10 (FEI Company, Eindhoven, The Netherlands). The images were digitally captured by SIS Megaview III CCD camera (FEI Company, Eindhoven, The Netherlands).

2.9. In vitro vascular differentiation

AAA-MSCs and h-MSCs were induced to vascular differentiation by treatment with vascular endothelial growth factor (VEGF) at 50 ng/mL for 7 days in MEM with 2% FBS. At the end of the exposure, cells were seeded on cover glasses at the density of 15.000 cells/glass, and incubated for 24 h. Then, the samples were fixed with 4% paraformaldehyde in phosphate buffer saline (PBS) containing 0.1 % Triton - X 100, at 4 °C and for 30 min, washed in PBS and treated with a solution of 2.5 % bovine serum albumin (BSA) (Sigma Aldrich, St. Louis, Missouri, USA) in PBS (blocking reagent) per 30 min at room temperature (RT).

Glasses were subsequently incubated over night at 4 °C with mouse anti-human CD31 antibody (Origene, Thermo Fisher Scientific, Monza, Italy). After several washes in PBS-T, the samples were incubated for 1 h
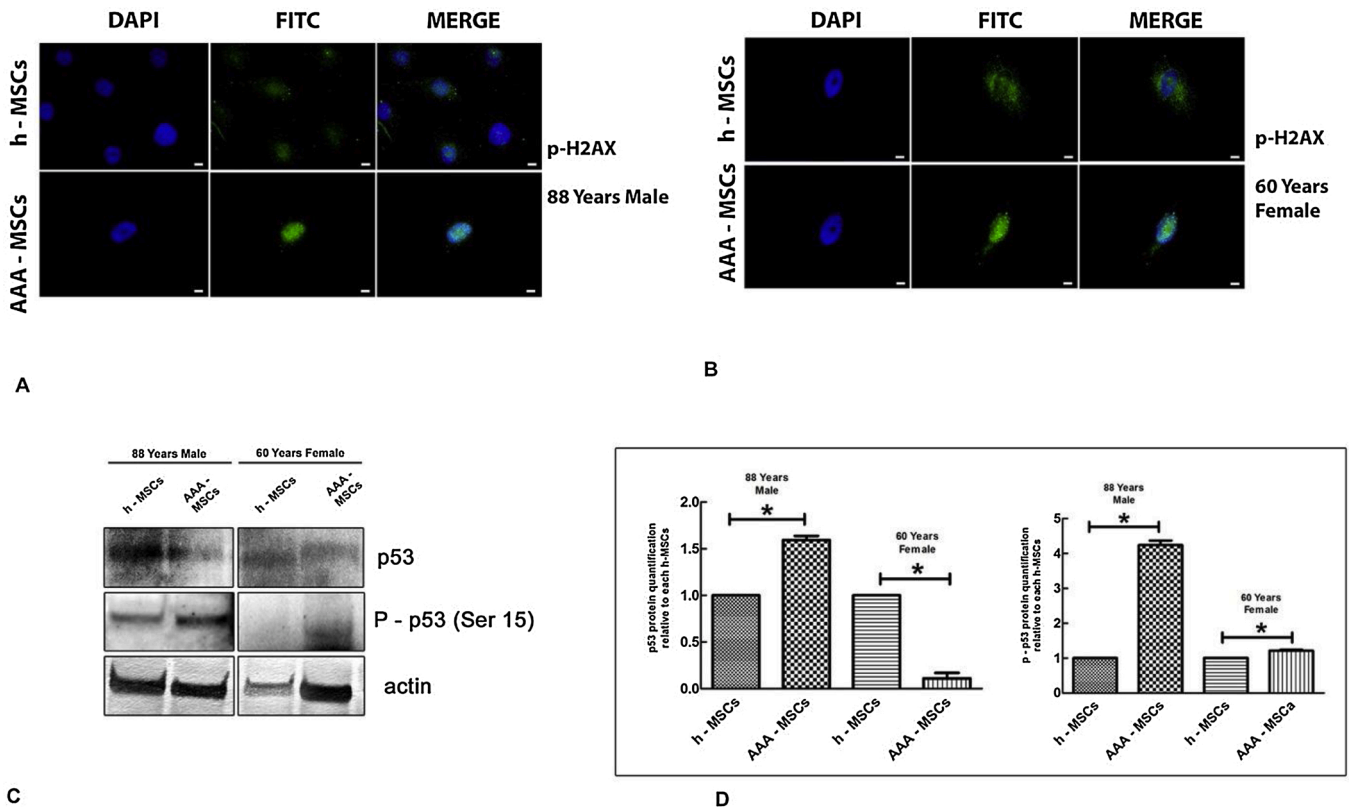

Fig. 5. (A and B) representative images of immunofluorescence labeling of p – H2AX in h – MSCs and AAA – MSCs isolated from two different donors. A FITC conjugated secondary antibody was used to detect the nuclear localization of p – H2AX. AAA – MSCs nuclei showed a stronger green fluorescent signal compared to h – MSCs nuclei (magnification 600X; bar: 100 nm); (C) representative western blot images showing total p53 and P-p53 protein expression in h – MSCs and AAA – MSCs. Results from two different donors were shown. (D) Relative amounts of total p53 and P-p53 protein expression were normalized to the intensity of actin and represented as fold increase relative to h – MSCs of each donor. Western blotting was performed in duplicate and the relative quantification was expressed as mean value ± SD. * represents a significant difference compared to h - MSCs, p < 0.05 (For interpretation of the references to colour in this figure legend, the reader is referred to the web version of this article).

and 30 min at 37 °C with secondary antibody anti- IgG – Cy3 conjugated (Sigma Aldrich, St. Louis, Missouri, USA), diluted 1:2000 in PBS. After rinsing in PBS the samples were counterstained with DAPI, mounted in vectashield medium (Vector Laboratories, Inc, Burlingame, CA, USA) and observed under a fluorescence microscopy Eclipse E800 Nikon (Nikon, Tokyo, Japan).

For the in vitro endothelial tube formation assay, after VEGF treatment, 1.5×10^3 cells were seeded onto a semi-solid matrix (Geltrex, Gibco, Thermo Fisher Scientific, Monza, Italy) at 37 °C, 5% CO_2 and incubated for 96 h. The formation of capillary networks was photographed under inverted light microscopy in a 10X magnification field.

2.10. Statistical analysis

Statistical analysis was carried out using GRAPH PAD PRISM 5.0 software (San Diego, CA, USA) applying a one-way ANOVA followed by Tukey's multiple comparison test. The differences were considered significant at $p < 0.05$.

3. Results

3.1. Mesenchymal surface marker expression in AAA – MSCs and h – MSCs

Fig. 1 shows the positive expression of CD105 and CD90 protein surface markers in both AAA – MSCs and h – MSCs in vitro cultured, and the lack of expression of CD14 and CD34 hematopoietic markers, demonstrating their classification as mesenchymal stromal cells, in agreement with the scientific literature (Dominici et al., 2006). The experiment was performed in cells isolated from all the patients with a positive signal corresponding to the expression of CD105 and CD90 proteins and a negative signal corresponding to the lack of expression of CD14 and CD34 proteins, in all the cells observed.

3.2. Cell proliferation assay

To demonstrate a difference in cell proliferation in AAA – MSCs and h – MSCs, a BrdU proliferation assay was carried out. Results showed a significant reduction in cellular proliferation in AAA – MSCs compared to h – MSCs (Fig. 2A), suggesting a block in cell growth in AAA – MSCs compatible with a cellular senescence state.

3.3. ROS detection

To detect a difference in the intracellular content of ROS in AAA – MSCs and h - MSCs, ROS detection assay was carried out. Results showed a significant increase of the total intracellular level of ROS in AAA – MSCs compared to h – MSCs (Fig. 2B), compatible with the presence of a high level of oxidative stress in aged and senescent cells.

3.4. vascular MSC surface area

In order to demonstrate a change in cellular shape and cell surface area in AAA – MSCs compared to h – MSCs, a F – actin staining assay was carried out. Fig. 3 showed the fluorescent signal corresponding to the actin protein and its distributions inside the cells. AAA – MSCs, (Fig. 3B) showed a large flat shape and a disorganization in the distribution of actin filaments into the cytoplasm, compared to h – MSCs (Fig. 3A) in which actin filaments are more parallel oriented. Quantitative analysis of cellular area showed AAA – MSCs with a cell surface area 2.4 folds higher compared to h – MSCs (Fig. 3C), in agreement with a senescent phenotype.

3.5. Cyclin-dependent kinase (CdK) inhibitor expression

In order to demonstrate an arrest of cell cycle in AAA – MSCs, the expression of CdK inhibitor markers p21^CIP1 and p16^INK4a was investigated. A strong protein expression of p21^CIP1 in AAA – MSCs was observed, compared to h – MSCs (Fig. 4A). Quantitative analysis demonstrated an upregulation of p21^CIP1 expression in AAA-MSCs compared to h-MSCs, ranging from 3 to 20 folds (Fig. 4B). On the contrary, the expression of p16^INK4a was significantly downregulated in AAA-MSCs compared to h – MSCs (Fig. 4D; E).

Immunofluorescence experiments confirmed a strong p21^CIP1 nuclear signal in AAA-MSCs compared to h-MSCs (Fig. 4C) and a weak p16^INK4a nuclear signal in AAA-MSCs compared to h-MSCs (Fig. 4F), consistent with the western blot results.

3.6. DNA damage response (DDR)

In order to verify the engagement of the DDR in AAA – MSCs, the expression of phosphorylated Histone H2AX, marker of activated DNA damage, was investigated. Fig. 5A and B showed a strong fluorescent signal in AAA-MSCs in both donors, while a weak signal was observed in h-MSCs, suggesting the activation of the DDR, consequence of a DNA damage, only in AAA-MSCs.

The persistence of DDR induces the phosphorylation and activation of the tumor suppressor protein p53. To this aim, the total p53 protein and the phosphorylated p53 protein (Ser 15) were investigated by western blot. The results showed a weak signal of total p53 protein in all the samples (Fig. 5C), while the phosphorylated p53 signal was higher in AAA-MSCs compared to h-MSCs (Fig. 5C), suggesting the activation of p53/p21^CIP1 pathway only in AAA - MSCs.

3.7. TEM analysis and autophagy

Autophagy is essential for the maintenance of cellular stemness and differentiation abilities. In order to demonstrate a dysfunctional autophagy in MSCs isolated from arterial wall, TEM analysis was carried out in combination with western blot analysis which investigate the expression of the autophagy-related marker Beclin1 and LC3 proteins.

Our results showed the presence of several autophagosomes and lysosomes in h – MSCs isolated from both donors, while their amount was significantly reduced in AAA – MSCs (Figure 6A and B). Western blot data confirmed a strong downregulation of Beclin-1 expression in AAA – MSCs compared to h-MSCs and a reduction of expression of LC3-I and LC3-II in AAA – MSCs compared to h-MSCs (Figure 6C and D), although there is a big difference between the donors tested.

3.8. CD31 immunolabeling and in vitro tubular assay

In order to demonstrate the ability of vascular MSCs to differentiate toward endothelial phenotype, immunolabeling for the endothelial marker CD31 was carried out after 7 days of in vitro VEGF stimulation. Results showed a high fluorescence signal corresponding to CD31 marker in h-MSCs compared to a weak signal in AAA – MSCs (Figure 7A), suggesting the lack of ability in AAA -MSCs to differentiate toward an endothelial phenotype.

In vitro tubular assay showed a spindle like morphology and tubular organization in h-MSCs treated with VEGF and then seeded on semi-solid matrix (Figure 7B), in agreement with an endothelial differentiation. On the contrary, AAA – MSCs exposed to VEGF and then seeded on semi-solid matrix showed a polygonal cellular shape (Figure 7B), suggesting the lack of endothelial differentiation. Control samples, consisting in h- MSCs and AAA – MSCs, not exposed to VEGF, and seeded on semi-solid matrix, showed a polygonal shape morphology (Figure 7B).
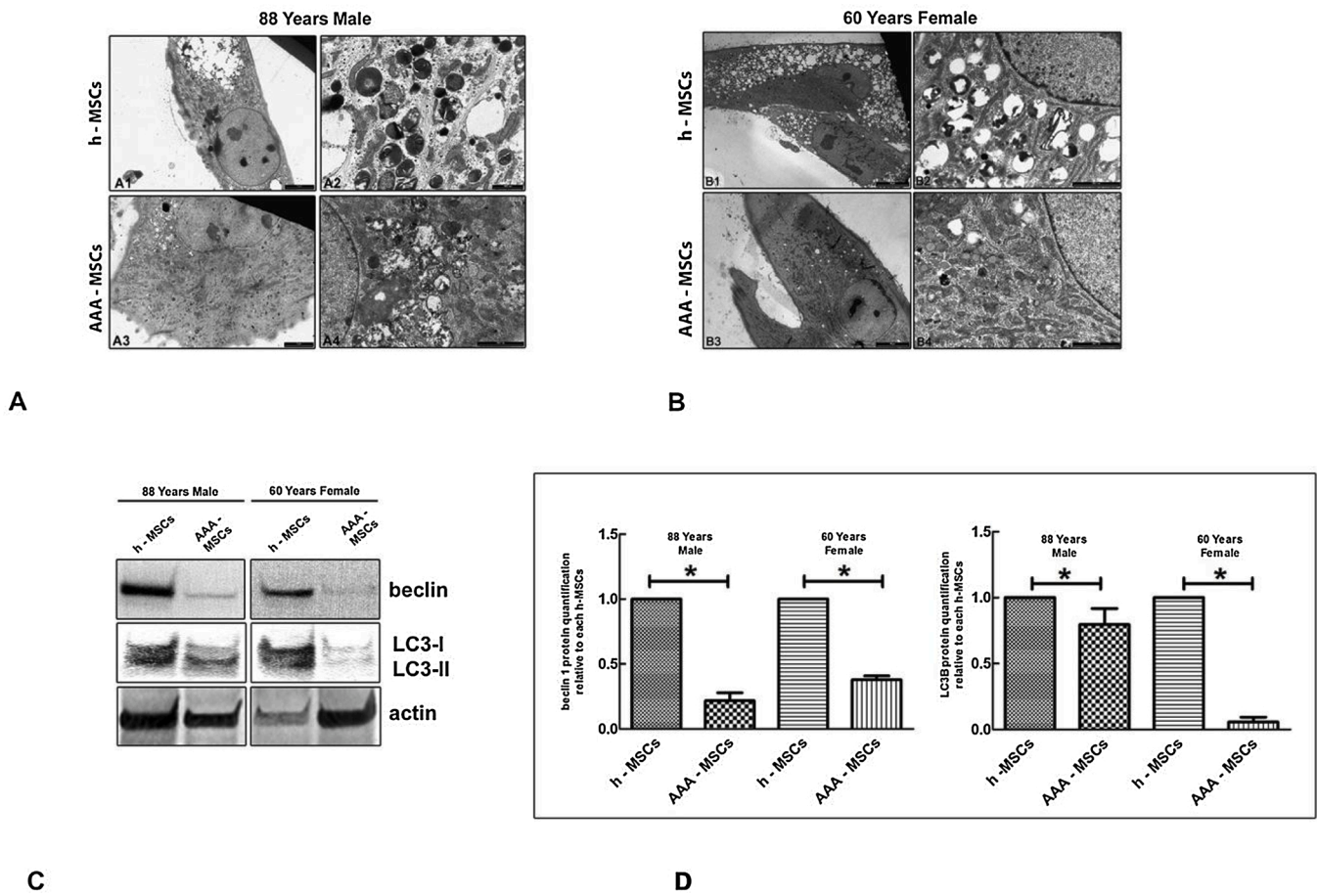
Fig. 6. TEM representative images showing h-MSCs, isolated from two donors (A- 88 years male; B – 60 years Female). (A1 and B1) low magnification images of h-MSCs showing the cytoplasm filled by the presence of several empty vesicles, lysosomes, secondary lysosomes, dense bodies and autophagosomes (A1 bar: 5 mm; A2 bar: 10 mm); (A2 and B2) detail of cytoplasm showing autophagosomes, primary and secondary lysosomes, dense bodies (bar A2: 1000 nm; bar B2: 2000 nm); (A3 and B3) low magnification images of AAA- MSCs showing the cytoplasm characterized by a reduced number of autophagosomes, primary and secondary lysosomes and dense bodies (A3 bar: 5 mm; B3 bar: 10 mm); (A4 and B4) high magnification image of AAA – MSCs showing a reduced number of autophagosomes, lysosomes and dense bodies in the cytoplasm (A4 bar: 2000 nm; B4 bar: 2000 nm). (C) western blot analysis showing the expression of autophagic related markers beclin1 and LC3 (LC3-I and LC3-II) in MSCs isolated from two different donors. (D) Relative amounts of beclin1 and LC3 (LC3-I and LC3-II) protein expression were normalized to the intensity of actin and represented as fold increase relative to h – MSCs. Each Western blot was performed in duplicate and the relative quantification was expressed as mean value $\pm$ SD. * represents a significant difference compared to h - MSCs, p < 0.05.

4. Discussion

The adult vascular wall is characterized by the presence of vascular progenitor cells which all have a key role in vessel repair and remodeling, during physiological and pathological conditions (Zhang et al., 2018; Lu and LI, 2018; Psaltis and Simari, 2015). Among them, the vascular MSCs are mainly localized in tunica media and adventitia of the vessels (Psaltis and Simari, 2015). In this study, vascular MSCs were isolated from aneurysmatic and healthy segments of abdominal aorta. Both cellular populations showed a positive staining for mesenchymal stromal markers, CD105 and CD90, and a negative staining for the CD14 and CD34 hematopoietic markers, demonstrating the ability to keep the mesenchymal phenotype in healthy and pathological conditions. Vascular MSCs, show the same properties of MSCs to differentiate toward vascular and non vascular cells (Veréb et al., 2020). In pathological conditions, resident vascular MSCs are actively involved in the progression of the disease, such as in releasing active MMP (Ciavarella et al., 2015) and as a source of calcyfing vascular cells and myofibroblasts, contributing to the development of atherosclerotic calcification (Zhang et al., 2018; Psaltis and Simari, 2015). The data reported in this study aim to demonstrate the presence of senescent vascular MSCs, isolated from the arterial wall of abnormal aneurysm, which could be involved in the onset and development of aneurysm disease.

Cellular senescence is a permanent growth arrest that promotes tissue remodeling during development and after injury. It also contributes to the decline of the regenerative potential and function of tissues in aged organisms (Hernandez-Seguira et al., 2018). An increased number of studies underlined a causative role of vascular senescent cells in the pathology of age-related diseases (Katsuumi et al., 2018). Indeed, senescent endothelial cells and vascular smooth muscle cells are found in the development and progression of atherosclerotic plaque (Katsuumi et al., 2018).

BrdU proliferation assay, carried out on vascular MSCs isolated from pathological and healthy segments of abdominal aorta, show a significant reduction in the proliferation of AAA-MSCs compared to h-MSCs, suggesting an arrest of cell cycle, in agreement with a senescent phenotype.

Furthermore, the increase of ROS level in AAA – MSCs compared to h – MSCs supported our hypothesis. Increased levels of ROS lead to oxidative stress which, in turn, could induce the DDR, telomere shortening, protein damage and mitochondrial dysfunction, all of which can contribute to cellular senescence in MSCs (Wang et al., 2020).

One of the main morphological changes connected with cellular senescence is the enlargement and irregularly shaped of the cell body, often linked to a rearrangement of the cytoskeleton proteins
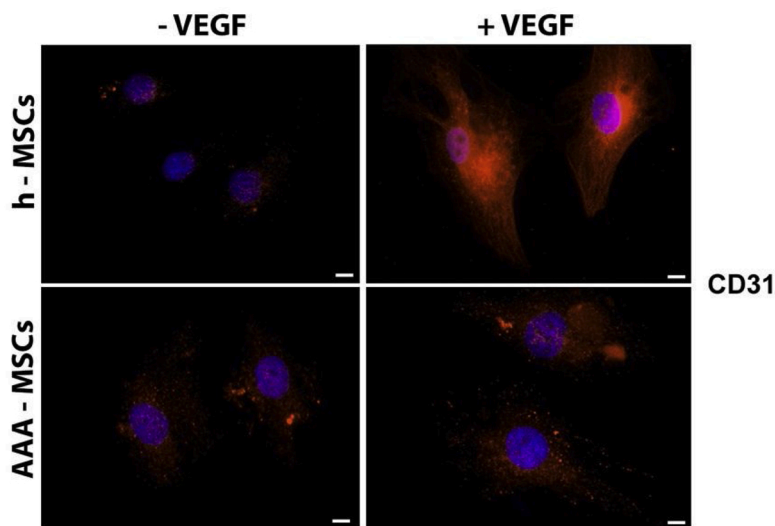
Fig. 7. (A) representative immunofluorescence images showing a high expression of the endothelial marker CD31 in h - MSCs and a low signal in AAA – MSCs. Both cell populations were in vitro exposed to VEGF for 7 days (+VEGF). Control samples consist in untreated cells (-VEGF). CY3 conjugated secondary antibody was used to detect the fluorescence signal. All the samples were counterstained with DAPI (magnification: 600X: bar: 100 nm). (B) In vitro tubular assay. h-MSCs and AAA -MSCs were exposed to VEGF for 7 days (+VEGF) and then seeded on semi-solid matrix for 3 days. A spindle like morphology and tubular organization, demonstrating an initial endothelial differentiation, was observed in h-MSCs. Untreated cells (- VEGF) represented control samples (magnification 50X; bar: 100 mm).
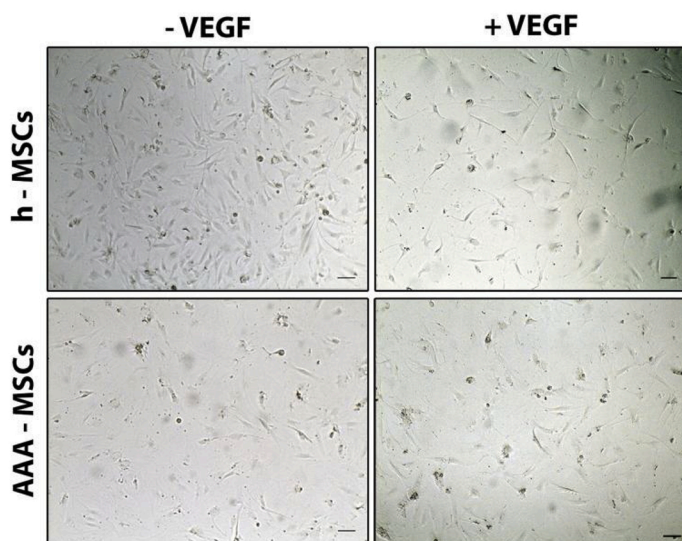
Hwang et al., 2009). Indeed, AAA – MSCs showed a large flat spread surface, with a 2.4 fold increase of the cell surface area compared to h – MSCs, in agreement with a senescent condition.

The results regarding a senescent state for AAA -MSCs are supported by the western blot and immunofluorescent data demonstrating a high expression of p21^{CIP1} CDKi in AAA-MSCs, in agreement with a G1 arrest in the cell cycle (Mijit et al., 2020; Hernandez-Seguira et al., 2018). On the other hand, the expression of the CDKi p16^{INK4a} shows an opposite signal, with higher expression in h-MSCs compared to AAA-MSCs. This apparently contradictory result reflects a condition of quiescent cells in h-MSCs compared to a senescent state in AAA-MSCs. According to Terzi and colleagues (2016), a quiescent phenotype is a reversible arrest of cell cycle characterized by a high expression level of p16^{INK4a}, connected

with low mitogen stimulation, while a senescent phenotype is characterized by high level of p21^{CIP1} expression, associated to a DNA damage and to the activation of DNA damage response (DDR).

It is widely considered P16^{INK4a} as the most common senescence marker (Sharpless and Sherr, 2015; He and Sharpless, 2017). Absent in unstressed, healthy tissues in young individuals, it is highly expressed in damaged and stressful conditions such as tumorigenesis, wounding and ageing (Sharpless and Sherr, 2015). Increases of P16^{INK4a} expression with chronological ageing has been also associated to hyporeplicative cells but not to the onset of age-related diseases such as osteoarthritis (Diekman et al., 2018).

In order to demonstrate a DDR response in AAA – MSCs, immuno-labeling for phosphorylated histone H2AX, marker of activated DNA

damage, was carried out. Results showed a spotted nuclear signal in AAA – MSCs, corresponding to phospho-H2AX nuclear foci. In presence of a DNA damage, cells active the DDR inducing senescence when the DNA damage is unresolved. Double strand DNA breaks promote the recruitment and binding of ATM kinase to the DNA damage site, which phosphorylates the histone H2AX, helping the assembly of specific DNA repair complex (Mijit et al., 2020; Hernandez-Seguira et al., 2018). The persistence of DDR induces the phosphorylation and activation of the tumor suppressor protein p53, which induces the transcription of several genes, included the locus CDKN2A encoding for the cyclin dependent kinase inhibitor p21^{CIP1} (Mijit et al., 2020; Bautista-Niño et al., 2016). In this study, a higher expression of phosphorylated p53 was showed in AAA – MSCs, confirming a block in cell cycle due to the activation of DDR, in agreement with the scientific literature.

It is well known that p53 can play alternative role in the regulation of metabolism, autophagy, DNA damage repair, cell cycle arrest, quiescence, senescence, and apoptosis. Indeed, factors such as p53 concentration, post-translational modifications, and microenvironment are responsible for inducing, through p53 activity, a precise pattern of genetic expression responsible of different cellular conditions (Mijit et al., 2020). The role of the pathway p53/ p21^{CIP1} in regulating cellular senescence by a DDR dependent response is one of the most important. p21^{CIP1} binds to and inhibits the activity of cyclin dependent kinases Cdk1 and Cdk2, and it is required for the p53-induced cell cycle arrest at either G1/S or G2/M checkpoints. Furthermore, it is reported that p21^{CIP1} binds many caspases, inhibiting apoptosis (Mijit et al., 2020). However, high doses of p53 following a severe DNA damage could lead to apoptosis, thus p53 concentrations seems to play a key role in determining cell fate (Chen et al., 2000). In our study, an increase of the phosphorylated p53 form was observed in AAA – MSCs isolated from both donors, suggesting the presence of a cellular senescent state. Anyway, a deeper investigation evaluating the correlation between p53 and apoptosis markers needs to be carried out to better clarify the role of p53 in regulating cellular senescence in the AAA.

The cellular senescence in vascular structure is called vascular senescence. There is evidence that vascular senescence is crucially involved in the pathogenesis of cardiovascular and metabolic disorders (Katssumi et al., 2018), such as in promoting atherosclerosis, systolic cardiac dysfunction, hypertension, intimal hyperplasia and diabetes (Katssumi et al., 2018). Cellular senescence is also responsible for the secretion of several pro-inflammatory factors which constitute the senescence-associated secretory phenotype (SAPS). SAPS makes an inflammatory microenvironment over time, which promotes the progression of several cardiovascular diseases (Machado-Oliveira et al., 2020).

It has been recently demonstrated that stem cells are characterized by the presence of constitutive autophagy, mechanism by which they keep their stemness (García-Prat et al., 2016). Once thought to be a cellular strategy to survive in stressful conditions, nowadays autophagy is described as an active mechanism to ensure renovation of intracellular components during homeostasis, keeping stem cells in a quiescence state to be rapidly activated upon an insult (García-Prat et al., 2016). Reduced autophagy has been associated with accelerated ageing and age-related diseases (Cheon et al., 2019; Mizushima and Levine, 2020). In our study, TEM analysis show the cytoplasm of h-MSCs largely filled by autophagic vesicles, lysosomes and dense bodies, while in AAA-MSC cytoplasm just a few autophagic vesicles are detected, suggesting a reduced autophagy. Western blot results confirmed a higher expression of Beclin and LC3 autophagic markers in h-MSCs compared to AAA-MSCs. In the cardiovascular system, autophagy has an essential role in heart and vessel homeostasis and function (Abdellatif et al., 2020; Gatica et al., 2015; Mialet-Perez and Vindis, 2017). A low level of constitutive autophagy is crucial for cardiac homestatis, allowing recycling and clearance of damaged proteins and organelles in cardiomyocytes, post mitotic cells which are not able to reduce their waste material by replication (Mialet-Perez and Vindis, 2017). With ageing, the autophagic activity becomes insufficient and a dysfunctional autophagy can arise, cooperating

in the development of the major cardiovascular diseases (Abdellatif et al., 2020; Mialet-Perez and Vindis, 2017). It has been suggested that a defective autophagy in endothelial and smooth muscle cells of the vascular wall may promote cellular senescence and/or cell death (Mialet-Perez and Vindis, 2017).

In order to evaluate the ability of vascular MSCs to in vitro differentiate toward an endothelial phenotype, AAA-MSCs and h-MSCs were exposed to VEGF and a vascular tubular assay was carried out. Results demonstrated a high expression of the endothelial marker CD31 and a spindle like morphology similar to tubular structure in h-MSCs compared to AAA-MSCs. These results suggest a reduced ability in senescent AAA-MSCs to differentiate toward a endothelial phenotype, in agreement with the scientific literature in which an impaired regenerative ability is demonstrated in senescent MSCs following a tissue damage (Cianflone et al., 2020; Di Micco et al., 2020).

5. Conclusions

Currently, the mortality associated with the rupture of AAA is still high and no medical therapies are so efficient in preventing it. Randomized clinical trials have demonstrated that the early surgical repair for small AAA is not beneficial (Golledge, 2019), so the development of drug based and/or cell based therapies is extremely urgent. Understanding the molecular mechanisms at the base of AAA onset and progression is mandatory to better develop specific drugs in preventing and /or treating it.

This study demonstrates the presence of senescent MSCs isolated from an aneurysmatic abdominal aorta which could be responsible for the development and progression of the disease. One limit of our investigation is the use of a few patients. To better clarify the relation between AAA and cellular senescence a high number of donors, also considering age, gender and AAA development grade, needs to be involved. Furthermore, a correlation between in vitro findings with abdominal aorta aneurysm explants is highly recommended to better elucidate the involvement of cellular senescence in the development of AAA. We hope this research will help to the development of therapeutical strategies targeting senescent cells and it could represent a valid intervention in preventing or delay age related pathologies.

Credit authorship contribution statement

Conceptualization **Gabriella Teti**, **Eleonora Mazzotti**, **Francesca Chiarini.**; methodology, **Eleonora Mazzotti**, **Gabriella Teti**, **Francesco Carano** and **Francesca Chiarini**; validation, **Mirella Falconi** and **Gabriella Teti**; investigation, **Eleonora Mazzotti**, **Gabriella Teti** and **Francesco Carano**; data curation, **Gabriella Teti** and **Alessandra Ruggeri**; writing—original draft preparation, **Gabriella Teti** and **Eleonora Mazzotti**; writing—review and editing, **Alessandra Ruggeri** and **Mirella Falconi**; Funding **Mirella Falconi** and **Alessandra Ruggeri**.

Funding

8. Declaration of Competing Interest

The authors report no declaration of interest.

Appendix A. Supplementary data

Supplementary material related to this article can be found, in the online version, at doi:https://doi.org/10.1016/j.mad.2021.111515.

References

Abdellatif, M., Ljubojevic-Holzer, S., Madeo, F., Sedej, S., 2020. Autophagy in cardiovascular health and disease. Prog. Mol. Biol. Transl. Sci. 172, 87–106. https://doi.org/10.1016/bs.pmbts.2020.04.022.

Ahangar, P., Mills, S.J., Cowin, A.J., 2020. Mesenchymal Stem Cell Secretome as an Emerging Cell-Free Alternative for Improving Wound Repair. Int. J. Mol. Sci. 21, 7038. https://doi.org/10.3390/ijms21197038.

Badger, S., Forster, R., Blair, P.H., Ellis, P., Kee, F., Harkin, D.W., 2017. Endovascular treatment for ruptured abdominal aortic aneurysm. Cochrane Database Syst. Rev. 5, CD005261 https://doi.org/10.1002/14651858.CD005261.pub4.

Ballard, D.J., Fowkes, F.G., Powell, J.T., 2000. Surgery for small asymptomatic abdominal aortic aneurysms. Cochrane Database Syst. Rev., CD001835 https://doi.org/10.1002/14651858.CD001835.

Banimohamad-Shotorbani, B., Kahroba, H., Sadeghzadeh, H., Wilson, D.M., Maadi, H., Samadi, N., Hejazi, M.S., Farajpour, H., Onari, B.N., Sadeghi, M.R., 2020. DNA damage repair response in mesenchymal stromal cells: from cellular senescence and aging to apoptosis and differentiation ability. Ageing Res. Rev. 62, 101125 https://doi.org/10.1016/j.arr.2020.101125.

Bautista-Niño, P.K., Portilla-Fernandez, E., Vaughan, D.E., Danser, A.H., Roks, A.J., 2016. DNA damage: a main determinant of vascular aging. Int. J. Mol. Sci. 17 https://doi.org/10.3390/ijms17050748.

Berlanga-Acosta, J.A., Guillén-Nieto, G.E., Rodríguez-Rodríguez, N., Mendoza-Mari, Y., Bringas-Vega, M.L., Berlanga-Saez, J.O., García Del Barco Herrera, D., Martinez-Jimenez, I., Hernandez-Gutierrez, S., Valdés-Sosa, P.A., 2020. Cellular senescence as the pathogenic hub of diabetes-related wound chronicity. Front. Endocrinol. (Lausanne) 11, 573032. https://doi.org/10.3389/fendo.2020.573032.

Bernal, S., Lopez-Sanz, L., Jimenez-Castilla, L., Prieto, I., Melgar, A., La Manna, S., Martin-Ventura, J.L., Blanco-Colio, L.M., Egido, J., Gomez-Guerrero, C., 2020. Protective effect of suppressor of cytokine signalling 1-based therapy in experimental abdominal aortic aneurysm. Br. J. Pharmacol. 178, 564–581. https://doi.org/10.1111/bph.15330.

Caplan, A.I., 2007. Adult mesenchymal stem cells for tissue engineering versus regenerative medicine. J. Cell. Physiol. 213, 341–347. https://doi.org/10.1002/jcp.21200.

Chen, Q.M., Liu, J., Merrett, J.B., 2000. Apoptosis or senescence-like growth arrest: influence of cell-cycle position, p53, p21 and bax in H2O2 response of normal human fibroblasts. Biochem. J. 347, 543. https://doi.org/10.1042/0264-6021:3470543.

Cheon, S.Y., Kim, H., Rubinsztein, D.C., Lee, J.E., 2019. Autophagy, cellular aging and age-related human diseases. Exp. Neurobiol. 28, 643–657. https://doi.org/10.5607/en.2019.28.6.643.

Cianflone, E., Torella, M., Biamonte, F., De Angelis, A., Urbanek, K., Costanzo, F.S., Rota, M., Ellison-Hughes, G.M., Torella, D., 2020. Targeting cardiac stem cell senescence to treat cardiac aging and disease. Cells 9. https://doi.org/10.3390/cells9061558.

Ciavarella, C., Alviano, F., Gallitto, E., Ricci, F., Buzzi, M., Velati, C., Stella, A., Freyrie, A., Pasquinelli, G., 2015. Human vascular wall mesenchymal stromal cells contribute to abdominal aortic aneurysm pathogenesis through an impaired immunomodulatory activity and increased levels of matrix Metalloproteinase-9. Circ. J. 79, 1460–1469. https://doi.org/10.1253/circj.CJ-14-0857.

Di Micco, R., Krizhanovsky, V., Baker, D., d'Adda di Fagagna, F., 2020. Cellular senescence in ageing: from mechanisms to therapeutic opportunities. Nat. Rev. Mol. Cell Biol. 22, 75–95. https://doi.org/10.1038/s41580-020-00314-w.

Diekman, B.O., Sessions, G.A., Collins, J.A., Knecht, A.K., Strum, S.L., Mitin, N.K., Carlson, C.S., Loeser, R.F., Sharpless, N.E., 2018. Expression of p16INK4a is a biomarker of chondrocyte aging but does not cause osteoarthritis. Aging Cell 17, e12771. https://doi.org/10.1111/acel.12771.

Dominici, M., Le Blanc, K., Mueller, I., Slaper-Cortenbach, I., Marini, F., Krause, D., Deans, R., Keating, A., Prockop, D., Horwitz, E., 2006. Minimal criteria for defining multipotent mesenchymal stromal cells. The International Society for Cellular Therapy position statement. Cytotherapy 8, 315–317. https://doi.org/10.1080/14653240600855905.

Focaroli, S., Teti, G., Salvatore, V., Durante, S., Belmonte, M.M., Giardino, R., Mazzotti, A., Bigi, A., Falconi, M., 2014. Chondrogenic differentiation of human adipose mesenchimal stem cells: influence of a biomimetic gelatin genipin crosslinked porous scaffold. Microsc. Res. Tech. 77, 928–934. https://doi.org/10.1002/jemt.22417.

Focaroli, S., Teti, G., Salvatore, V., Orienti, I., Falconi, M., 2016. Calcium/Cobalt alginate beads as functional scaffolds for cartilage tissue engineering. Stem Cells Int. 2016, 2030478 https://doi.org/10.1155/2016/2030478.

García-Prat, L., Martínez-Vicente, M., Perdiguero, E., Ortet, L., Rodríguez-Ubreva, J., Rebollo, E., Ruiz-Bonilla, V., Gutarra, S., Ballestar, E., Serrano, A.L., Sandri, M., Muñoz-Cánoves, P., 2016. Autophagy maintains stemness by preventing senescence. Nature 529, 37–42. https://doi.org/10.1038/nature16187.

Gatica, D., Chiong, M., Lavandero, S., Klionsky, D.J., 2015. Molecular mechanisms of autophagy in the cardiovascular system. Circ. Res. 116, 456–467. https://doi.org/10.1161/CIRCRESAHA.114.303788.

Golledge, J., 2019. Abdominal aortic aneurysm: update on pathogenesis and medical treatments. Nat. Rev. Cardiol. 16, 225–242. https://doi.org/10.1038/s41569-018-0114-9.

Harrell, C.R., Jovicic, B.P., Djonov, V., Volarevic, V., 2020. Therapeutic potential of mesenchymal stem cells and their secretome in the treatment of SARS-CoV-2-Induced acute respiratory distress syndrome. Anal Cell Pathol (Amst, 1939768. https://doi.org/10.1155/2020/1939768.

He, S., Sharpless, N.E., 2017. Senescence in health and disease. Cell 169, 1000–1011. https://doi.org/10.1016/j.cell.2017.05.015.

Hernandez-Segura, A., Nehme, J., Demaria, M., 2018. Hallmarks of cellular senescence. Trends Cell Biol. 28, 436–453. https://doi.org/10.1016/j.tcb.2018.02.001.

Hwang, E.S., Yoon, G., Kang, H.T., 2009. A comparative analysis of the cell biology of senescence and aging. Cell. Mol. Life Sci. 66, 2503–2524. https://doi.org/10.1007/s00018-009-0034-2.

Jia, G., Aroor, A.R., Jia, C., Sowers, J.R., 2019. Endothelial cell senescence in aging-related vascular dysfunction. Biochim Biophys Acta Mol Basis Dis. 1865, 1802–1809. https://doi.org/10.1016/j.bbadis.2018.08.008.

Katsuumi, G., Shimizu, I., Yoshida, Y., Minamino, T., 2018. Vascular senescence in cardiovascular and metabolic diseases. Front. Cardiovasc. Med. 5, 18. https://doi.org/10.3389/fcvm.2018.00018.

López-Otín, C., Blasco, M.A., Partridge, L., Serrano, M., Kroemer, G., 2013. The hallmarks of aging. Cell 153, 1194–1217. https://doi.org/10.1016/j.cell.2013.05.039.

Lu, W., Li, X., 2018. Vascular stem/progenitor cells: functions and signaling pathways. Cell. Mol. Life Sci. 75, 859–869. https://doi.org/10.1007/s00018-017-2662-2.

Lunyak, V.V., Amaro-Ortiz, A., Gaur, M., 2017. Mesenchymal stem cells secretory responses: senescence messaging secretome and immunomodulation perspective. Front. Genet. 8, 220. https://doi.org/10.3389/fgene.2017.00220.

Machado-Oliveira, G., Ramos, C., Marques, A.R.A., Vieira, O.V., 2020. Cell senescence, multiple organelle dysfunction and atherosclerosis. Cells 9, 2146. https://doi.org/10.3390/cells9102146.

Mattioli-Belmonte, M., Teti, G., Salvatore, V., Focaroli, S., Orciani, M., Dicarlo, M., Fini, M., Orsini, G., Di Primio, R., Falconi, M., 2015. Stem cell origin differently affects bone tissue engineering strategies. Front. Physiol. 6, 266. https://doi.org/10.3389/fphys.2015.00266.

Mazzotti, E., Teti, G., Falconi, M., Chiarini, F., Barboni, B., Mazzotti, A., Muttini, A., 2019. Age-related alterations affecting the chondrogenic differentiation of synovial fluid mesenchymal stromal cells in an equine model. Cells 8, 1116. https://doi.org/10.3390/cells8101116.

McCarthy, C.G., Wenceslau, C.F., Webb, R.C., Joe, B., 2019. Novel contributors and mechanisms of cellular senescence in hypertension-associated premature vascular aging. Am. J. Hypertens. 32, 709–719. https://doi.org/10.1093/ajh/hpz052.

Mialet-Perez, J., Vindis, C., 2017. Autophagy in health and disease: focus on the cardiovascular system. Essays Biochem. 61, 721–732. https://doi.org/10.1042/EBC20170022.

Mijit, M., Caracciolo, V., Melillo, A., Amicarelli, F., Giordano, A., 2020. Role of p53 in the regulation of cellular senescence. Biomolecules. 10, 420. https://doi.org/10.3390/biom10030420.

Mizushima, N., Levine, B., 2020. Autophagy in human diseases. N. Engl. J. Med. 383, 1564–1576. https://doi.org/10.1056/NEJMra2022774.

Mohammad, K., Dakik, P., Medkour, Y., Mitrofanova, D., Titorenko, V.I., 2019. Quiescence entry, maintenance, and exit in adult stem cells. Int. J. Mol. Sci. 20 https://doi.org/10.3390/ijms20092158.

Peshkova, I.O., Schaefer, G., Koltsova, E.K., 2016. Atherosclerosis and aortic aneurysm - is inflammation a common denominator? FEBS J. 283, 1636–1652. https://doi.org/10.1111/febs.13634.

Psaltis, P.J., Simari, R.D., 2015. Vascular wall progenitor cells in health and disease. Circ. Res. 116, 1392–1412. https://doi.org/10.1161/CIRCRESAHA.116.305368.

Psaltis, P.J., Harbuzariu, A., Delacroix, S., Holroyd, E.W., Simari, R.D., 2011. Resident vascular progenitor cells–diverse origins, phenotype, and function. J. Cardiovasc. Transl. Res. 4, 161–176. https://doi.org/10.1007/s12265-010-9248-9.

Regulski, M.J., 2017. Cellular senescence: what, why, and how. Wounds 29, 168–174.

Schmitz-Rixen, T., Keese, M., Hakimi, M., Peters, A., Böckler, D., Nelson, K., Grundmann, R.T., 2016. Ruptured abdominal aortic aneurysm-epidemiology, predisposing factors, and biology. Langenbecks Arch. Surg. 401, 275–288. https://doi.org/10.1007/s00423-016-1401-8.

Sharpless, N.E., Sherr, C.J., 2015. Forging a signature of in vivo senescence. Nat. Rev. Cancer 2015 (15), 397–408. https://doi.org/10.1038/nrc3960.

Shimizu, I., Minamino, T., 2019. Cellular senescence in cardiac diseases. J. Cardiol. 74, 313–319. https://doi.org/10.1016/j.jjcc.2019.05.002.

So, W.K., Cheung, T.H., 2018. Molecular regulation of cellular quiescence: a perspective from adult stem cells and its niches. Methods Mol. Biol. 1686, 1–25. https://doi.org/10.1007/978-1-4939-7371-2_1.

Terzi, M.Y., Izmirli, M., Gogebakan, B., 2016. The cell fate: senescence or quiescence. Mol. Biol. Rep. 43, 1213–1220. https://doi.org/10.1007/s11033-016-4065-0.

Teti, G., Cavallo, C., Grigolo, B., Giannini, S., Facchini, A., Mazzotti, A., Falconi, M., 2012. Ultrastructural analysis of human bone marrow mesenchymal stem cells during in vitro osteogenesis and chondrogenesis. Microsc. Res. Tech. 75, 596–604. https://doi.org/10.1002/jemt.21096.

Teti, G., Focaroli, S., Salvatore, V., Mazzotti, E., Ingra', L., Mazzotti, A., Falconi, M., 2018. The hypoxia-mimetic agent cobalt chloride differently affects human mesenchymal stem cells in their chondrogenic potential. Stem Cells Int. 2018, 3237253 https://doi.org/10.1155/2018/3237253.

Ungvari, Z., Tarantini, S., Donato, A.J., Galvan, V., Csiszar, A., 2018. Mechanisms of vascular aging. Circ. Res. 123, 849–867. https://doi.org/10.1161/CIRCRESAHA.118.311378.

Ungvari, Z., Tarantini, S., Sorond, F., Merkely, B., Csiszar, A., 2020. Mechanisms of vascular aging, a geroscience perspective: JACC focus seminar. J. Am. Coll. Cardiol. 75, 931–941. https://doi.org/10.1016/j.jacc.2019.11.061.

Veréb, Z., Mázló, A., Szabó, A., Póliska, S., Kiss, A., Litauszky, K., Koncz, G., Boda, Z., Rajnavölgyi, É., Bácsi, A., 2020. Vessel wall-derived mesenchymal stromal cells share similar differentiation potential and immunomodulatory properties with bone marrow-derived stromal cells. Stem Cells Int. 2020, 8847038 https://doi.org/10.1155/2020/8847038.

Wang, Y., Liu, Y., Chen, E., Pan, Z., 2020. The role of mitochondrial dysfunction in mesenchymal stem cell senescence. Cell Tissue Res. 382, 457–462. https://doi.org/10.1007/s00441-020-03272-z.

Zhang, L., Issa Bhaloo, S., Chen, T., Zhou, B., Xu, Q., 2018. Role of resident stem cells in vessel formation and arteriosclerosis. Circ. Res. 122, 1608–1624. https://doi.org/10.1161/CIRCRESAHA.118.313058.